The Astrophysical Journal, 844:97 (10pp), 2017 August 1 https://doi.org/10.3847/1538-4357/aa7a15

Polarized Line Formation in Arbitrary Strength Magnetic Fields Angle-averaged and Angle-dependent Partial Frequency Redistribution

M. Sampoorna[1], K. N. Nagendra[1], and J. O. Stenflo[2,3]
[1] Indian Institute of Astrophysics, Koramangala, Bengaluru 560 034, India; sampoorna@iiap.res.in, knn@iiap.res.in
[2] Institute of Astronomy, ETH Zurich, CH-8093 Zurich, Switzerland; stenflo@astro.phys.ethz.ch
[3] Istituto Ricerche Solari Locarno, via Patocchi, CH-6605 Locarno-Monti, Switzerland
Received 2017 May 4; revised 2017 June 16; accepted 2017 June 16; published 2017 July 26

Abstract

Magnetic fields in the solar atmosphere leave their fingerprints in the polarized spectrum of the Sun via the Hanle and Zeeman effects. While the Hanle and Zeeman effects dominate, respectively, in the weak and strong field regimes, both these effects jointly operate in the intermediate field strength regime. Therefore, it is necessary to solve the polarized line transfer equation, including the combined influence of Hanle and Zeeman effects. Furthermore, it is required to take into account the effects of partial frequency redistribution (PRD) in scattering when dealing with strong chromospheric lines with broad damping wings. In this paper, we present a numerical method to solve the problem of polarized PRD line formation in magnetic fields of arbitrary strength and orientation. This numerical method is based on the concept of operator perturbation. For our studies, we consider a two-level atom model without hyperfine structure and lower-level polarization. We compare the PRD idealization of angle-averaged Hanle–Zeeman redistribution matrices with the full treatment of angle-dependent PRD, to indicate when the idealized treatment is inadequate and what kind of polarization effects are specific to angle-dependent PRD. Because the angle-dependent treatment is presently computationally prohibitive when applied to realistic model atmospheres, we present the computed emergent Stokes profiles for a range of magnetic fields, with the assumption of an isothermal one-dimensional medium.

Key words: line: profiles – polarization – radiative transfer – scattering – Sun: atmosphere

1. Introduction

The regime of strong (kilogauss) magnetic fields where the Zeeman effect dominates is a well explored topic over a long period of time in solar magnetic field diagnostics (see the review by Stenflo 2013). In recent years, the regime of weak (milligauss to few tens of Gauss) magnetic fields where the Hanle effect dominates is also quite well explored (Stenflo 1994; Landi Degl'Innocenti & Landolfi 2004; Stenflo 2013). However, the regime of intermediate fields (hecto-Gauss fields like 50–500 Gauss for optical lines), is relatively less explored. This is because in this regime both the Hanle and Zeeman effects contribute significantly and hence have to be treated simultaneously in the formulation and solution of the concerned polarized radiative transfer equation. Such a problem of polarized line formation in the intermediate field regime becomes numerically complex when partial frequency redistribution (PRD) in scattering is taken into account.

A first numerical solution for this problem was presented in Sampoorna et al. (2008), where a perturbation method (similar to that of Nagendra et al. 2002) was proposed to solve the concerned polarized transfer equation. However, the perturbation method, wherein polarization is treated as a perturbation to intensity, works well only for smaller degrees of polarization. For larger degrees of polarization, direct numerical methods such as the Feautrier method (see, e.g., Dumont et al. 1977; Faurobert 1987) and discrete space method (see, e.g., Nagendra 1986, 1988) would be required. However, these classical methods are computationally expensive for complex polarized transfer problems, like the ones described above. Therefore, it is more advantageous to work with iterative techniques that provide accurate solutions at a much higher computational speed. A comparison of the direct methods and the iterative methods are given in Nagendra et al. (1999).

In the last few decades the iterative methods based on the concept of operator perturbation (Cannon 1973) have been applied to solve a variety of polarized transfer problems (see the reviews by Trujillo Bueno 2003; Nagendra 2017). In the present paper, we apply this operator perturbation technique to solve the problem of polarized PRD line formation in arbitrary strength magnetic fields. In order to make the treatment computationally tractable, here we consider an isothermal one-dimensional planar atmosphere, and a two-level atom model with zero nuclear spin and infinitely sharp lower level. We neglect lower-level polarization. The Hanle–Zeeman redistribution matrix corresponding to scattering on such a two-level atom is derived in Bommier (1997a, 1997b) using a rigorous QED approach, in Bommier & Stenflo (1999) using a classical oscillator theory, and in Sampoorna (2011) using the Kramers–Heisenberg scattering approach of Stenflo (1994). The equivalence between these theoretical approaches is shown in Sampoorna et al. (2007a, 2007b) for a $J = 0 \rightarrow 1 \rightarrow 0$ scattering transition and in Sampoorna (2011) for a $J_l \rightarrow J_u \rightarrow J_l$ scattering transition (where J's denote the total angular momentum quantum number).

More recently, this problem has also been addressed by Alsina Ballester et al. (2017) for the approximation of an angle-averaged Hanle–Zeeman PRD matrix. An important result by these authors (see also Alsina Ballester et al. 2016) is that, in strong resonance lines for which the effects of PRD are significant, the magneto-optical terms of the Stokes-vector transfer equation produce a clear magnetic sensitivity in the wings of the Q/I profile, as well as sizable U/I wing signals that are also sensitive to the presence of magnetic fields with strengths similar to or larger than those needed for the onset of

the Hanle effect in the spectral line under consideration. Recently, we have pointed out that in the presence of weak magnetic fields the angle-dependent PRD effects cannot be neglected (see Nagendra et al. 2002; Nagendra & Sampoorna 2011; Supriya et al. 2013; Sampoorna 2014). Therefore, in the present paper, we consider both the angle-averaged and angle-dependent Hanle–Zeeman redistribution matrices and study the validity of the angle-averaged approximation for not only the Hanle regime but also the intermediate regime of field strengths.

The paper is organized as follows. In Section 2, we briefly present the basic equations governing the problem at hand. The numerical method of the solution is described in Section 3. The emergent Stokes profiles for different field strengths, and angle-averaged and angle-dependent cases are presented in Section 4. Conclusions are presented in Section 5. In Appendices A and B, we present the Hanle–Zeeman redistribution matrix and Zeeman line absorption matrix in the atmospheric reference frame. Appendix C presents the normalization of the Hanle–Zeeman redistribution matrix.

2. The Basic Equations

In the presence of a magnetic field, the polarized radiative transfer equation for the Stokes vector $\boldsymbol{I}(\tau, x, \boldsymbol{n}) = (I, Q, U, V)^{\mathrm{T}}$ may be written as

$$\mu \frac{\partial}{\partial \tau}\boldsymbol{I}(\tau, x, \boldsymbol{n}) = \boldsymbol{K}\boldsymbol{I}(\tau, x, \boldsymbol{n}) - \boldsymbol{S}(\tau, x, \boldsymbol{n}), \tag{1}$$

where τ is the line-center optical depth, $x = (\nu_0 - \nu)/\Delta\nu_{\mathrm{D}}$ is the frequency separation from line center ν_0 in Doppler width ($\Delta\nu_{\mathrm{D}}$) units, the vector $\boldsymbol{n}(\vartheta, \varphi)$ is the propagation direction of the ray (where ϑ is the co-latitude and φ the azimuth), and $\mu = \cos\vartheta$. The absorption matrix $\boldsymbol{K}$ is given by

$$\boldsymbol{K} = \boldsymbol{\Phi} + r\boldsymbol{E}, \tag{2}$$

where $\boldsymbol{\Phi}$ is the 4×4 Zeeman line absorption matrix, $\boldsymbol{E}$ is the 4×4 unity matrix, and r is the ratio of continuous to line-center opacity. The source vector is given by

$$\boldsymbol{S}(\tau, x, \boldsymbol{n}) = (r\boldsymbol{E} + \epsilon\,\boldsymbol{\Phi})B_{\nu_0}\boldsymbol{U} + \boldsymbol{S}_{\mathrm{scat}}(\tau, x, \boldsymbol{n}), \tag{3}$$

where

$$\boldsymbol{S}_{\mathrm{scat}}(\tau, x, \boldsymbol{n}) = \oint \frac{d\boldsymbol{n}'}{4\pi}\int_{-\infty}^{+\infty} dx' \boldsymbol{R}(x, \boldsymbol{n}; x', \boldsymbol{n}'; \boldsymbol{B})\boldsymbol{I}(\tau, x', \boldsymbol{n}'). \tag{4}$$

In Equation (3), ϵ denotes the photon destruction probability per scattering, B_{ν_0} is the Planck function, and $\boldsymbol{U} = (1, 0, 0, 0)^{\mathrm{T}}$. The redistribution matrix $\boldsymbol{R}(x, \boldsymbol{n}; x', \boldsymbol{n}'; \boldsymbol{B})$ accounts for the correlations in frequency, angle, and polarization between the incident radiation field at frequency x' and direction $\boldsymbol{n}'$ and the reemitted radiation at frequency x and direction $\boldsymbol{n}$ in the presence of a vector magnetic field $\boldsymbol{B}$. The quantity $d\boldsymbol{n}'$ is an element of solid angle around $\boldsymbol{n}'$. The explicit form of the Hanle–Zeeman redistribution matrix $\boldsymbol{R}$ and the Zeeman line absorption matrix $\boldsymbol{\Phi}$ are given in Appendices A and B respectively.

Let us define a total optical depth $d\tau^{\mathrm{tot}} = d\tau(\varphi_I + r)/\mu$, where φ_I is the diagonal element of the Zeeman line absorption matrix $\boldsymbol{\Phi}$. For notational simplification, here we will call $d\tau^{\mathrm{tot}} = d\tau$. Equation (1) can then be rewritten as

$$\frac{\partial}{\partial \tau}\boldsymbol{I}(\tau, x, \boldsymbol{n}) = \boldsymbol{I}(\tau, x, \boldsymbol{n}) - \boldsymbol{S}_{\mathrm{eff}}(\tau, x, \boldsymbol{n}). \tag{5}$$

Here the effective source vector is

$$\boldsymbol{S}_{\mathrm{eff}}(\tau, x, \boldsymbol{n}) = \boldsymbol{S}_{\mathrm{tot}}(\tau, x, \boldsymbol{n}) - \boldsymbol{K}'\boldsymbol{I}(\tau, x, \boldsymbol{n}), \tag{6}$$

where we have redefined the total absorption matrix of Equation (2) as

$$\boldsymbol{K}' = \frac{\boldsymbol{K}}{(\varphi_I + r)} - \boldsymbol{E}. \tag{7}$$

The total source vector is defined as

$$\boldsymbol{S}_{\mathrm{tot}}(\tau, x, \boldsymbol{n}) = \frac{\boldsymbol{S}(\tau, x, \boldsymbol{n})}{(\varphi_I + r)}. \tag{8}$$

The formal solution of Equation (5) is obtained by using the DELOPAR method of Trujillo Bueno (2003, see also Sampoorna et al. 2008).

3. Numerical Method of the Solution

Here we present an iterative method based on the concept of operator perturbation to solve Equation (5). Hereafter, we omit the τ dependence of the quantities, while their angle-frequency dependences appear as subscripts. The formal solution of Equation (5) can be written in terms of the lambda operator as

$$\boldsymbol{I}_{x\boldsymbol{n}} = \boldsymbol{\Lambda}_{x\boldsymbol{n}}[\boldsymbol{S}_{\mathrm{eff},x\boldsymbol{n}}]. \tag{9}$$

Following Olson et al. (1986), we define a local, "angle-frequency dependent" approximate lambda operator $\boldsymbol{\Lambda}^*_{x\boldsymbol{n}}$ through

$$\boldsymbol{\Lambda}_{x\boldsymbol{n}} = \boldsymbol{\Lambda}^*_{x\boldsymbol{n}} + (\boldsymbol{\Lambda}_{x\boldsymbol{n}} - \boldsymbol{\Lambda}^*_{x\boldsymbol{n}}). \tag{10}$$

We can now set up an iterative scheme to compute the effective source vector as

$$\boldsymbol{S}^{n+1}_{\mathrm{eff},x\boldsymbol{n}} = \boldsymbol{S}^{n}_{\mathrm{eff},x\boldsymbol{n}} + \delta\boldsymbol{S}^{n}_{\mathrm{eff},x\boldsymbol{n}}, \tag{11}$$

where the superscript n refers to the nth iteration step. From Equation (6), we find that

$$\delta\boldsymbol{S}^{n}_{\mathrm{eff},x\boldsymbol{n}} = \delta\boldsymbol{S}^{n}_{\mathrm{tot},x\boldsymbol{n}} - \boldsymbol{K}'\delta\boldsymbol{I}^{n}_{x\boldsymbol{n}}. \tag{12}$$

For numerical simplicity, we neglect the $\delta\boldsymbol{I}^{n}_{x\boldsymbol{n}}$ term, and obtain from Equations (8) and (3)

$$\delta\boldsymbol{S}^{n}_{\mathrm{eff},x\boldsymbol{n}} = \frac{\delta\boldsymbol{S}^{n}_{\mathrm{scat},x\boldsymbol{n}}}{\varphi_{I,x\boldsymbol{n}} + r}. \tag{13}$$

Substituting Equations (6), (8), and (3) in Equations (11) and (13), it is easy to find that

$$\boldsymbol{S}^{n+1}_{\mathrm{scat},x\boldsymbol{n}} = \boldsymbol{S}^{n}_{\mathrm{scat},x\boldsymbol{n}} + \delta\boldsymbol{S}^{n}_{\mathrm{scat},x\boldsymbol{n}}. \tag{14}$$

Combining Equations (9)–(14) with Equation (4), we derive an expression for $\delta\boldsymbol{S}^{n}_{\mathrm{scat},x\boldsymbol{n}}$ as

$$\delta\boldsymbol{S}^{n}_{\mathrm{scat},x\boldsymbol{n}} - \oint \frac{d\boldsymbol{n}'}{4\pi}\int_{-\infty}^{+\infty} dx' \frac{\boldsymbol{R}_{x\boldsymbol{n},x'\boldsymbol{n}',\boldsymbol{B}}}{\varphi_{I,x'\boldsymbol{n}'} + r}\boldsymbol{\Lambda}^*_{x'\boldsymbol{n}'}[\delta\boldsymbol{S}^{n}_{\mathrm{scat},x'\boldsymbol{n}'}] = [\boldsymbol{S}^{n}_{\mathrm{scat},x\boldsymbol{n}}]_{\mathrm{FS}} - \boldsymbol{S}^{n}_{\mathrm{scat},x\boldsymbol{n}}, \tag{15}$$

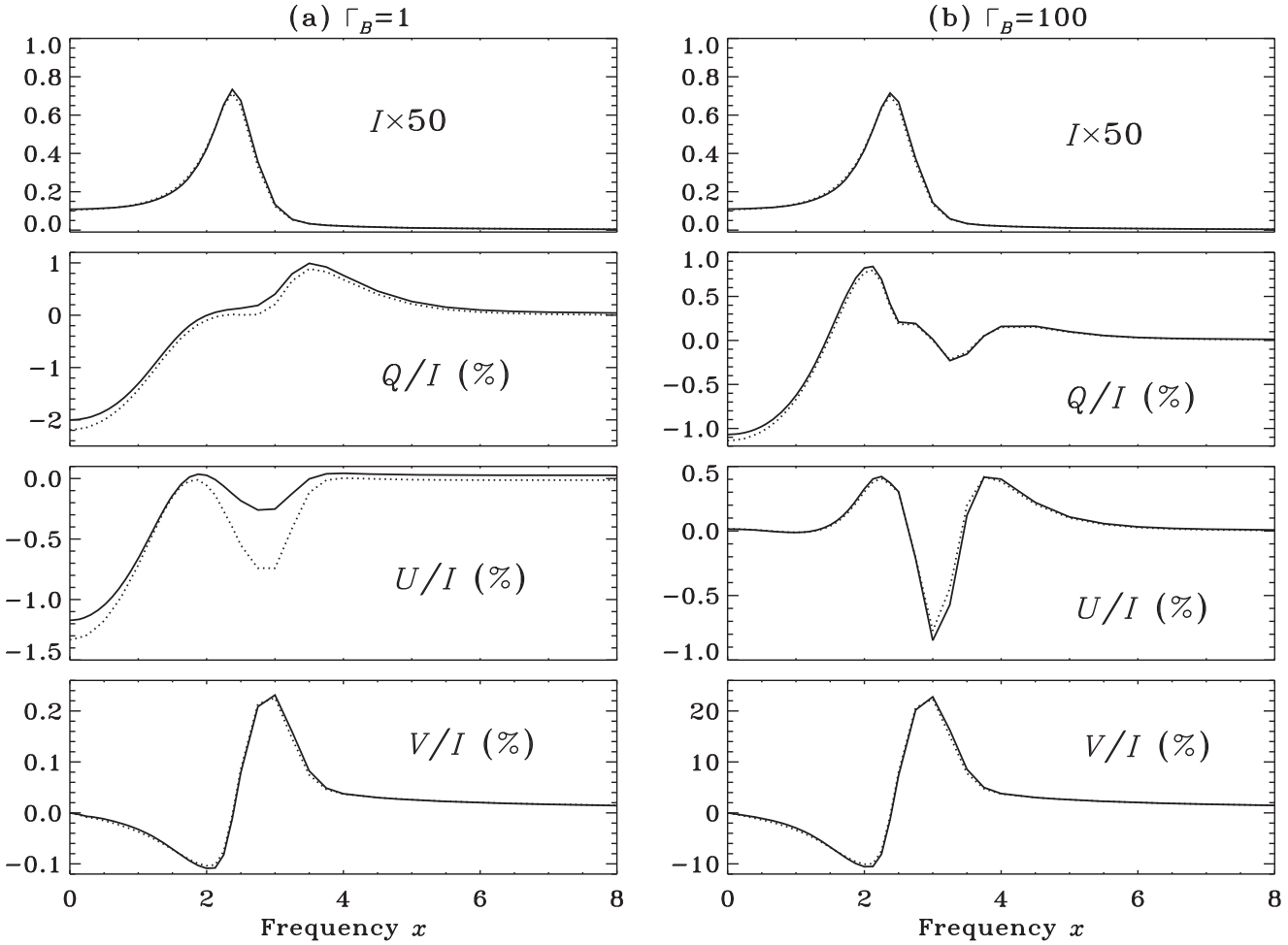

Figure 1. Comparison of emergent Stokes profiles computed using angle-dependent type-II and type-III redistribution functions (dotted lines) and those using angle-dependent type-II and CRD functions (solid lines). The line of sight is at $\mu = 0.11$ and $\varphi = 0°$. An isothermal self-emitting slab is considered with the following model parameters: (T, a, ϵ, r, Γ_E/Γ_R) = (200, 10^{-3}, 10^{-4}, 10^{-9}, 1); and magnetic field orientations: (ϑ_B, φ_B) = (30°, 0°). Panel (a) corresponds to $\Gamma_B = 1$ and panel (b) to $\Gamma_B = 100$.

where

$$[\boldsymbol{S}^n_{\mathrm{scat},x\boldsymbol{n}}]_{\mathrm{FS}} = \oint \frac{d\boldsymbol{n}'}{4\pi} \int_{-\infty}^{+\infty} dx' \boldsymbol{R}_{x\boldsymbol{n},x'\boldsymbol{n}',\boldsymbol{B}} \boldsymbol{\Lambda}_{x'\boldsymbol{n}'} [\boldsymbol{S}^n_{\mathrm{eff},x'\boldsymbol{n}'}], \quad (16)$$

is obtained from a formal solution of the effective source vector $\boldsymbol{S}_{\mathrm{eff},x\boldsymbol{n}}$ of the previous iterate. The system of Equations (15) can be rewritten in the form

$$\boldsymbol{A}\delta\boldsymbol{S}^n_{\mathrm{scat}} = \boldsymbol{r}^n, \quad (17)$$

where residual vector $\boldsymbol{r}^n$ is given by the right-hand side of Equation (15). At each depth point, $\delta\boldsymbol{S}^n_{\mathrm{scat}}$ and $\boldsymbol{r}^n$ are vectors of length $4N_x\, 2N_\mu\, N_\varphi$, where N_x is the number of frequency points in the range of $[0, x_{\max}]$, N_μ is the number of angle points in the range $[0 < \mu \leqslant 1]$, and N_φ is the number of azimuth points in the range $[0 \leqslant \varphi \leqslant 2\pi]$. The matrix $\boldsymbol{A}$ thus has dimensions $(4N_x\, 2N_\mu\, N_\varphi \times 4N_x\, 2N_\mu\, N_\varphi)$ at each depth point. It is computationally formidable to compute this huge matrix and then invert it. Thus it is necessary to find a work around for this problem.

Following Trujillo Bueno & Manso Sainz (1999, see also Alsina Ballester et al. 2017), we apply the approximate lambda iteration technique only to the intensity component of the source vector, i.e., S_I, because it drives the convergence rate. Other polarization components of the source vector are computed by the classical lambda iteration method, but with the important difference that the Stokes I parameter on which these components depend is being improved in the previous iteration by applying the approximate lambda iteration scheme to S_I. In this case, Equation (15) simplifies to

$$\delta S^n_{I,\mathrm{scat},x\boldsymbol{n}} - \oint \frac{d\boldsymbol{n}'}{4\pi} \int_{-\infty}^{+\infty} dx' \frac{\boldsymbol{R}_{00,x\boldsymbol{n},x'\boldsymbol{n}',\boldsymbol{B}}}{\varphi_{I,x'\boldsymbol{n}'} + r} \Lambda^*_{x'\boldsymbol{n}'} [\delta S^n_{I,\mathrm{scat},x'\boldsymbol{n}'}] = [S^n_{I,\mathrm{scat},x\boldsymbol{n}}]_{\mathrm{FS}} - S^n_{I,\mathrm{scat},x\boldsymbol{n}}, \quad (18)$$

for the intensity component of the source vector. It is important to note that $[S^n_{I,\mathrm{scat},x\boldsymbol{n}}]_{\mathrm{FS}}$ is the intensity component of $[\boldsymbol{S}^n_{\mathrm{scat},x\boldsymbol{n}}]_{\mathrm{FS}}$, which is obtained from the formal solution of the effective source vector $\boldsymbol{S}_{\mathrm{eff},x\boldsymbol{n}}$ of the previous iterate. Thus the coupling of other Stokes parameters to Stokes I is retained in the computation of $[S^n_{I,\mathrm{scat},x\boldsymbol{n}}]_{\mathrm{FS}}$. However, this coupling is neglected in the computation of the second term in the left-hand side of Equation (18), to reduce the computational cost. Again Equation (18) can be written in a form similar to Equation (17), but now the length of the residual vector and source vector correction is $N_x\, 2N_\mu\, N_\varphi$ and correspondingly the dimension of the $\boldsymbol{A}$ matrix is $(N_x\, 2N_\mu\, N_\varphi \times N_x\, 2N_\mu\, N_\varphi)$ at each depth point. With this

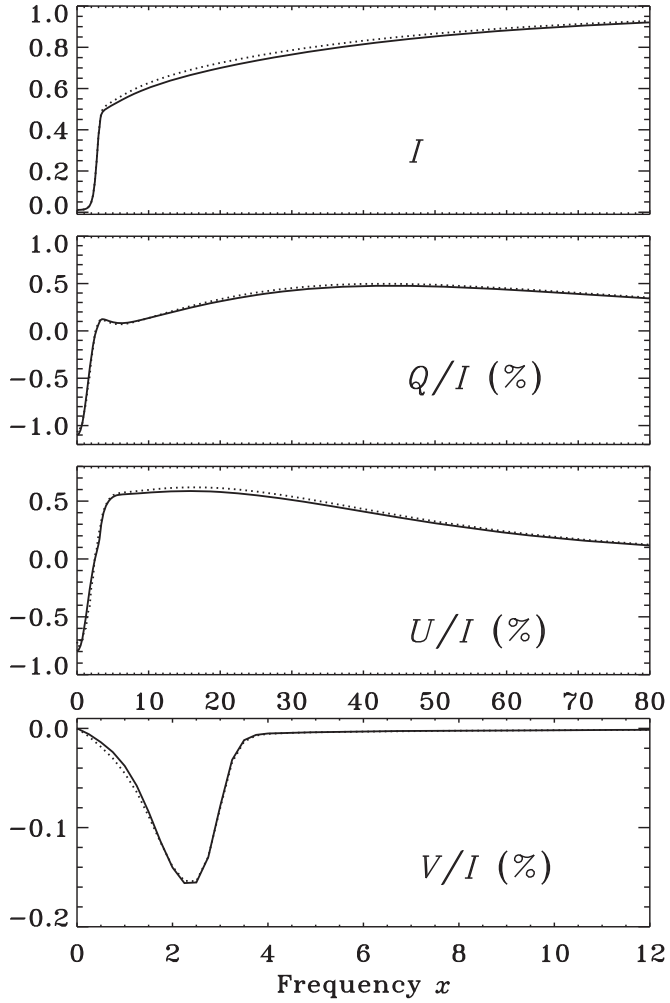

Figure 2. Comparison of emergent Stokes profiles computed using angle-dependent type-II and type-III redistribution functions (dotted lines) and those using angle-dependent type-II and CRD functions (solid lines). The line of sight is at $\mu = 0.11$ and $\varphi = 0°$. An isothermal semi-infinite atmosphere is considered with the following model parameters: $(T, a, \epsilon, r, \Gamma_E/\Gamma_R) = (10^9, 10^{-3}, 10^{-4}, 10^{-7}, 1)$; and magnetic field parameters: $(\Gamma_B, \vartheta_B, \varphi_B) = (1, 90°, 45°)$.

simplification, the problem becomes computationally feasible. We find that the numerical method presented in this section converges well for field strengths up to 300 G.

4. Results and Discussions

We consider isothermal, plane-parallel atmospheres with either no incident radiation at the boundaries (self-emitting slabs) or semi-infinite atmospheres with Planck function radiation field incident on the lower boundary (typical of optically thick stellar atmospheres). Such slab models are characterized by $(T, a, \epsilon, r, \Gamma_E/\Gamma_R)$, where T is the optical thickness of the slab. The Planck function at the line center B_{ν_0} is taken as unity. The depolarizing elastic collision parameter is assumed to be $D^{(1)} = D^{(2)} = 0.5\Gamma_E$, while $D^{(0)} = 0$. The magnetic field parameters are $(\Gamma_B, \vartheta_B, \varphi_B)$, where $\Gamma_B = g_{J_u}\omega_L/\Gamma_R$ and angles (ϑ_B, φ_B) define the field orientation with respect to the atmospheric normal. We use a logarithmic depth grid with five points per decade. The first depth point is at $\tau_1 = 10^{-4}$. For the frequency grid, we use equally spaced points in the line core and logarithmically spaced ones in the wings. Furthermore, the maximum frequency $x_{\max}$ is chosen such that the monochromatic optical thickness at $x_{\max}$ is much smaller than unity. We typically have 70 points in the interval $[0, x_{\max}]$. We use a seven-point Gaussian quadrature in $[0 < \mu \leqslant 1]$ and an eight-point trapezoidal grid for $0 \leqslant \varphi \leqslant 2\pi$. We consider a two-level atom model with $J_l = 0$ and $J_u = 1$. To obtain accurate solution, particularly for the case of angle-dependent redistribution functions, it is necessary to correctly normalize the Hanle–Zeeman redistribution matrix. This aspect is discussed in more detail in Appendix C.

4.1. Validity of Approximating the Type-III Redistribution Function by CRD

From Equations (31)–(34), it is clear that the numerical evaluation of type-III redistribution functions is computationally expensive because it involves evaluating an integral. Therefore, in the literature, the type-III redistribution function is often approximated by the complete frequency redistribution (CRD) function. The validity of this approximation for the computation of intensity is discussed in detail in Mihalas (1978). In this section, we present the validity of this approximation for polarization.

For the problem at hand, the above-mentioned approximation implies approximating the magnetic redistribution functions of type-III by

$$
\begin{aligned}
R^{\mathrm{III,HH}}_{M_u M_l, M'_u M'_l}(x, x', \Theta) &= H(a, x'_{M_u M_l}) H(a, x_{M'_u M'_l}),\\
R^{\mathrm{III,HF}}_{M_u M_l, M'_u M'_l}(x, x', \Theta) &= H(a, x'_{M_u M_l}) F(a, x_{M'_u M'_l}),\\
R^{\mathrm{III,FH}}_{M_u M_l, M'_u M'_l}(x, x', \Theta) &= F(a, x'_{M_u M_l}) H(a, x_{M'_u M'_l}),\\
R^{\mathrm{III,FF}}_{M_u M_l, M'_u M'_l}(x, x', \Theta) &= F(a, x'_{M_u M_l}) F(a, x_{M'_u M'_l}).
\end{aligned}
\tag{19}
$$

Figures 1 and 2 show a comparison of emergent Stokes profiles computed using the angle-dependent type-II and type-III redistribution functions (dotted lines) and those using angle-dependent type-II and CRD functions (solid lines). For optically thin self-emitting slabs, small differences are noticed in Q/I and U/I for weak fields (see Figure 1(a)). However, these differences reduce and nearly vanish as the field strength increases (see Figure 1(b)). This may be due to the increasing dominance of the Zeeman effect with an increase in field strength. Intensity and circular polarization are nearly identical for both the cases. For semi-infinite atmospheres, the approximation of replacing the type-III redistribution function by CRD does not seem to produce any noticeable effect on the emergent Stokes profiles already for weak fields (see Figure 2). Therefore, replacing the type-III redistribution function by CRD (see Equations (19)) is a good approximation not only for the computation of intensity but also for the computation of polarized profiles in arbitrary field strengths. From here on we use this approximation for all the illustrations presented in the rest of the paper.

4.2. Effect of Anomalous Dispersion Coefficients on Emergent Stokes Profiles

In Zeeman effect theory, the anomalous dispersion coefficients χ_i (see Equation (42)) are known to play a significant role in the emergent Stokes profiles only for strong fields (see, e.g., Stenflo 1994; Landi Degl'Innocenti & Landolfi 2004). However, in the case of optically thick scattering lines, these coefficients are shown to play a significant role already for fields that are in the Hanle regime (see Alsina Ballester et al. 2017). In this section, we

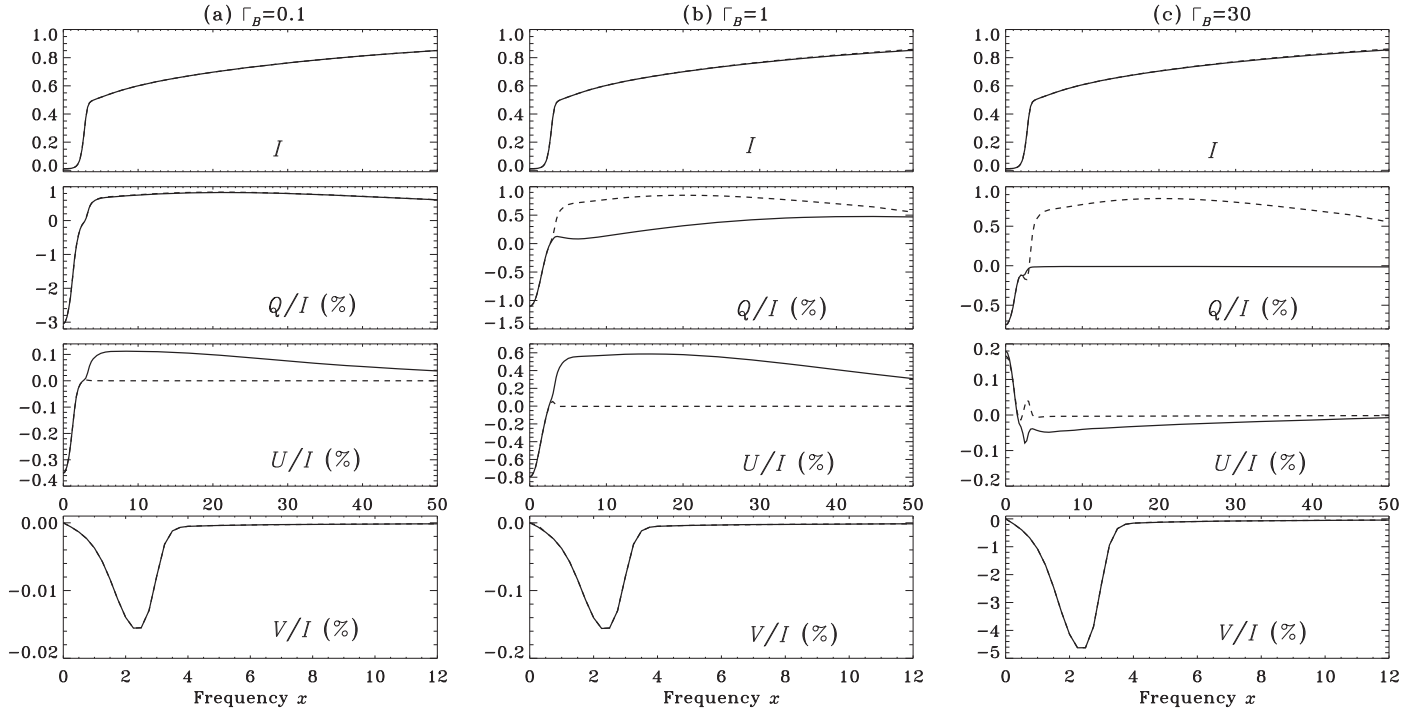

Figure 3. Effect of anomalous dispersion coefficients on emergent Stokes profiles computed using angle-dependent Hanle–Zeeman redistribution matrix. The line of sight is at $\mu = 0.11$ and $\varphi = 0°$. An isothermal semi-infinite atmosphere is considered with the following model parameters: $(T, a, \epsilon, r, \Gamma_E/\Gamma_R) = (10^9, 10^{-3}, 10^{-4}, 10^{-7}, 1)$; and magnetic field orientations: $(\vartheta_B, \varphi_B) = (90°, 45°)$. Panel (a) corresponds to $\Gamma_B = 0.1$, panel (b) to $\Gamma_B = 1$, and panel (c) to $\Gamma_B = 30$. The solid line is computed including the anomalous dispersion coefficients in the Zeeman absorption matrix, while the dashed line is computed by neglecting these coefficients.

re-confirm their finding, but now for the case of angle-dependent Hanle–Zeeman redistribution matrix.

Figure 3 shows a comparison of emergent Stokes profiles computed including (solid lines) and neglecting (dashed lines) the anomalous dispersion coefficients in the Zeeman absorption matrix. Even for very weak fields ($\Gamma_B = 0.1$), we see significant differences between the two cases, particularly in the wings of the U/I profiles. Indeed, all of the wing signatures in U/I are entirely due to the anomalous dispersion coefficients (particularly due to the χ_V coefficient that couples the Stokes Q and the U). As the field strength increases, the effect of these coefficients are also seen in the wings of Q/I. We remark that these wing signatures are not directly caused by the PRD functions or the Hanle effect. Indeed, the PRD is responsible for the generation of Q/I signals in the line wings, which are modified subsequently by the χ_V coefficient to give rise to the full magnetic sensitivity noticed in the wings of Q/I and U/I profiles. The intensity and V/I on the other hand do not show much sensitivity to these coefficients for the magnetic field parameters considered in Figure 3.

4.3. Stokes Profiles Computed with the Angle-dependent and Angle-averaged Hanle–Zeeman PRD Matrix

The solution of the polarized transfer equation, including angle-dependent PRD functions is known to be computationally very expensive. To avoid such computationally expensive problems, it is often a common practice to replace the angle-dependent PRD functions by their angle-averaged versions (see, e.g., Rees & Saliba 1982; Faurobert 1987; Nagendra et al. 2002). For the problem at hand, the angle-averaged approximation implies replacing the angle-dependent magnetic redistribution functions defined in Equations (29)–(34) by their angle-averaged counterparts, which are defined as

$$\bar{R}^{\rm II,\,X}_{M_l' M_u M_l}(x, x') = \frac{1}{2}\int_0^\pi R^{\rm II,\,X}_{M_l' M_u M_l}(x, x', \Theta)\sin\Theta d\Theta, \quad (20)$$

$$\bar{R}^{\rm III,\,XY}_{M_u M_l, M_u' M_l'}(x, x') = \frac{1}{2}\int_0^\pi R^{\rm III,\,XY}_{M_u M_l, M_u' M_l'}(x, x', \Theta) \times \sin\Theta d\Theta, \quad (21)$$

where X and Y stand for the symbols H and/or F.

We have studied the validity of the angle-averaged approximation as a function of field strength. For this, we considered the case of an isothermal semi-infinite atmosphere and varied the field strength parameter Γ_B from 0.1 to 100. We recall that, the damping parameter a is given by

$$a = \frac{\Gamma_R + \Gamma_I + \Gamma_E}{4\pi\Delta\nu_{\rm D}}. \quad (22)$$

For a spectral line at 5000 Å, a typical Doppler width of 30 mÅ, a damping parameter $a = 10^{-3}$, and $\Gamma_E/\Gamma_R = 1$, we obtain from Equation (22) $\Gamma_R = 2.26 \times 10^7$ s^{-1} (where we have assumed $\Gamma_I/\Gamma_R \ll 1$). In terms of the field strength B in Gauss, $\Gamma_B = 0.88 \times 10^7 g_{J_u}(B/\Gamma_R)$. For a $J = 0 \rightarrow 1 \rightarrow 0$ scattering transition considered for the illustrations presented in this paper, the Landé factor of the upper level $g_{J_u} = 1$. Clearly, a variation of Γ_B between 0.1 and 100, then corresponds to a variation in the range between 0.25 and 256 G in field strength.

Figures 4 and 5 show a comparison of the emergent Stokes profiles computed with the angle-dependent (solid lines) and angle-averaged (dashed lines) Hanle–Zeeman redistribution matrix for different values of the field strength parameter Γ_B. For optically thick lines, the differences between the two cases are seen mainly in the line core region (which is in agreement

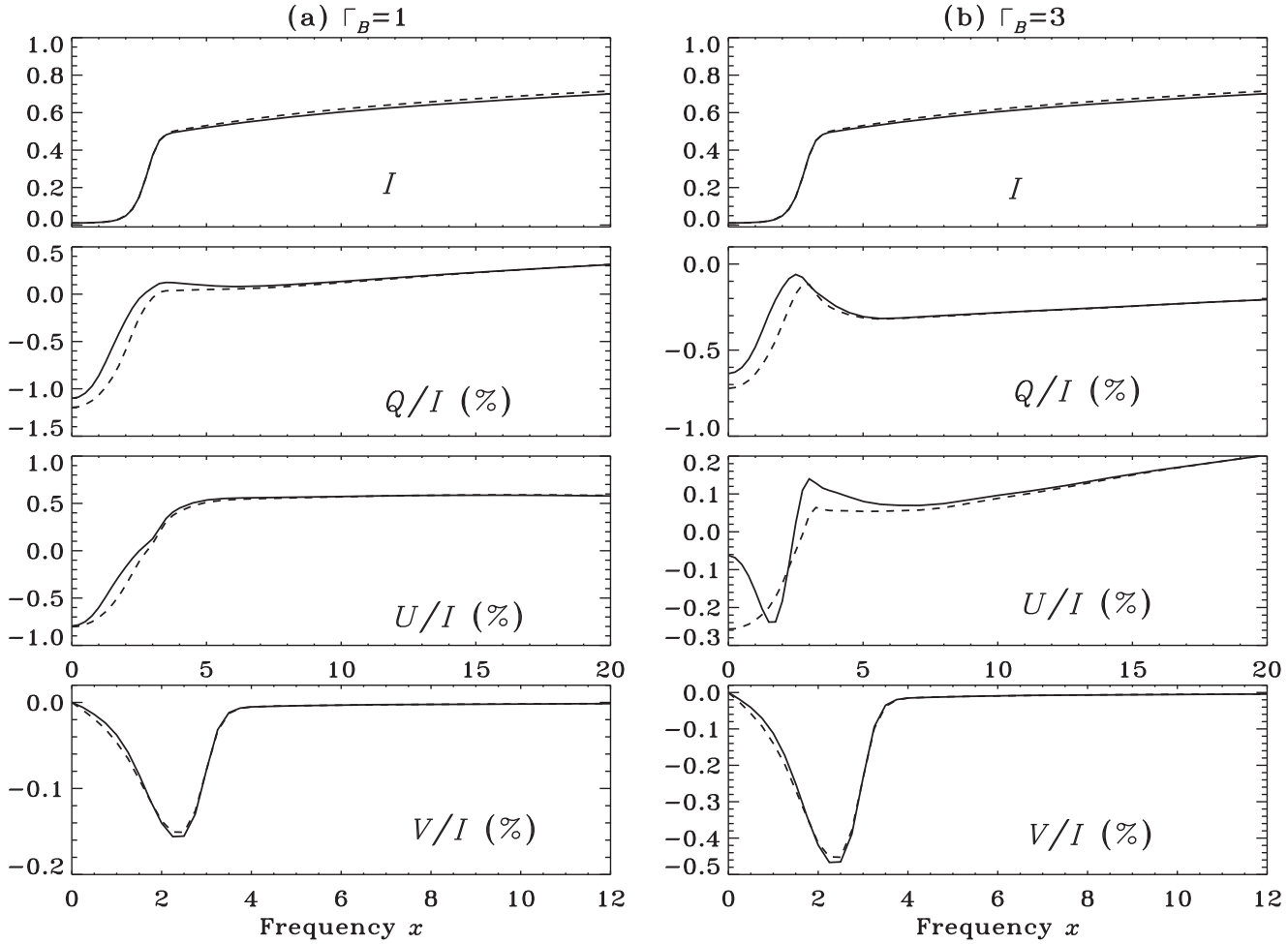

Figure 4. Comparison of emergent Stokes profiles computed using an angle-dependent (solid lines) and those using an angle-averaged (dashed lines) Hanle–Zeeman redistribution matrix. The line of sight is at $\mu = 0.11$ and $\varphi = 0°$. An isothermal semi-infinite atmosphere is considered with the following model parameters: $(T, a, \epsilon, r, \Gamma_E/\Gamma_R) = (10^9, 10^{-3}, 10^{-4}, 10^{-7}, 1)$; and magnetic field orientations: $(\vartheta_B, \varphi_B) = (90°, 45°)$. Panel (a) corresponds to $\Gamma_B = 1$, and panel (b) to $\Gamma_B = 3$.

with the results presented in Figure 6(b) of Nagendra & Sampoorna 2011). The intensity and the V/I profiles are insensitive to the choice of angle-dependent or angle-averaged functions, while the linear polarization profiles are considerably sensitive. From Figures 4 and 5, we see that the differences between the U/I profiles computed with angle-dependent and angle-averaged PRD functions are particularly large for the Hanle saturation regime field strength represented by $\Gamma_B = 3$. The differences between the two cases continue to persist for fields in the intermediate Hanle–Zeeman regime and for Γ_B as large as 100. This shows that angle-dependent effects are important for the computation of linear polarization profiles, particularly the U/I profiles.

5. Conclusions

In the present paper, we consider the problem of polarized line formation including the effects of PRD and magnetic fields of arbitrary strength and orientation. We consider scattering on a two-level atom with zero nuclear spin and an infinitely sharp unpolarized lower level. The Hanle–Zeeman redistribution matrix corresponding to this case has been derived in Bommier (1997a, 1997b, see also Bommier & Stenflo 1999; Sampoorna et al. 2007a, 2007b; Sampoorna 2011). We have developed an iterative technique based on the concept of operator perturbation to solve the concerned polarized radiative transfer equation. Unlike the perturbation method presented in Sampoorna et al. (2008), the present numerical method is robust and is able to handle atmospheres with any total optical thickness. However, like the perturbation method, the present method converges well for field strengths up to 300 G. This is due to the fact that the operator perturbation technique has been applied only for the computation of source vector corresponding to the intensity component of the Stokes vector. Although the operator perturbation technique can be applied to all four Stokes parameters, it becomes computationally impractical to implement the same in reality.

We have performed numerical studies to analyze the importance of the angle-dependent Hanle–Zeeman PRD matrix in the computation of the emergent Stokes profiles of optically thick lines, for a range of field strength parameters Γ_B between 0.1 and 100. In agreement with the previous studies for the case of the weak field (Nagendra & Sampoorna 2011), we find that the angle-dependent effects are significant mainly in the line core and particularly for the computation of linear polarization profiles. Significant differences between the U/I profiles computed with angle-dependent and angle-averaged PRD functions are noticed for fields in the saturation regime of the Hanle effect. The differences in both Q/I and U/I persist for fields as large as $\Gamma_B = 100$. Therefore, we conclude that angle-dependent effects are important and should be taken into

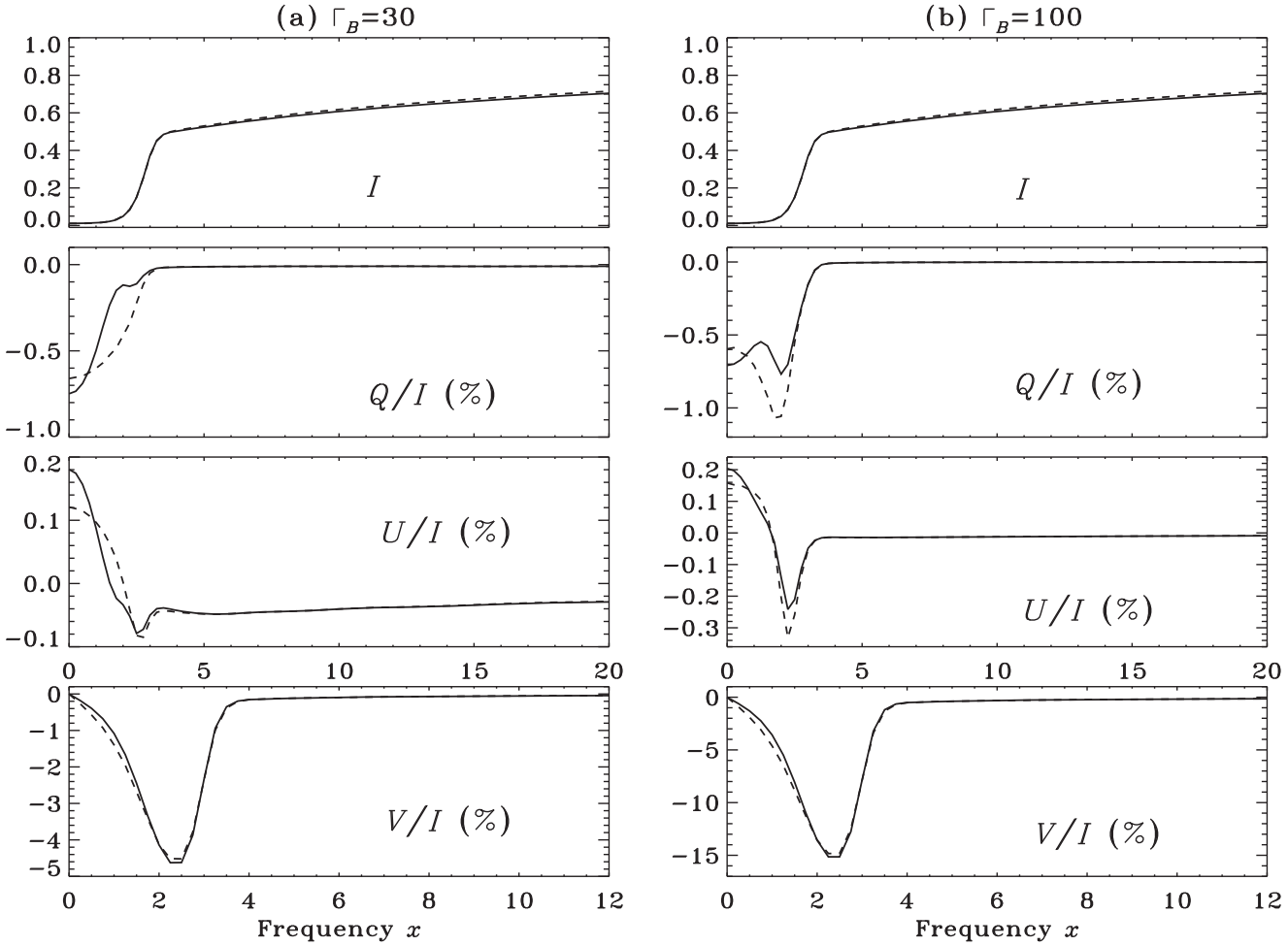

Figure 5. Same as Figure 4, but for $\Gamma_B = 30$ in panel (a) and $\Gamma_B = 100$ in panel (b).

account for an accurate determination of the magnetic field. Furthermore, we have shown that the approximation of replacing the angle-dependent type-III PRD functions by CRD is a good approximation for optically thick lines. Finally, we re-confirm the importance of anomalous dispersion coefficients of the Zeeman absorption matrix on producing interesting signatures in the wings of linear polarization profiles even for very weak fields (as originally shown in Alsina Ballester et al. 2017).

We thank an anonymous referee for constructive comments that helped improve the paper. Computations are performed on a 20 node HYDRA cluster (dual Xeon X5675 with 6 cores per processor and 3.06 GHz clock speed), FORNAX (dual opteron 6220 with 8 cores and 3.0 GHz clock speed), and KASPAR (dual Xeon X5675 with 6 cores per processor and 3.06 GHz clock speed) computing facilities at the Indian Institute of Astrophysics.

Appendix A
The Hanle–Zeeman Redistribution Matrix

The Hanle–Zeeman redistribution matrix derived in Bommier (1997b, see also Sampoorna et al. 2007a, 2007b; Sampoorna 2011) refers to a frame where the magnetic field is along the Z-axis (namely, the magnetic reference frame: MRF). However, for transfer computations, we need this matrix defined in a frame where the Z-axis is along the atmospheric normal (namely, the atmospheric reference frame: ARF). Transformation between the two frames is described in Appendix D of Sampoorna et al. (2007b), where this transformation is performed numerically. On the other hand, the same transformation can be expressed in a more compact analytic form by using the irreducible spherical tensors for polarimetry introduced by Landi Degl'Innocenti (1984). The latter is presented in this Appendix.

For a $J_l \rightarrow J_u \rightarrow J_l$ scattering transition with infinitely sharp lower level J_l, the Hanle–Zeeman redistribution matrix is given by (see Equation (48) of Bommier 1997b)

$$\boldsymbol{R}(x, \boldsymbol{n}; x', \boldsymbol{n}'; \boldsymbol{B}) = \boldsymbol{R}^{\rm II}(x, \boldsymbol{n}; x', \boldsymbol{n}'; \boldsymbol{B}) + \boldsymbol{R}^{\rm III}(x, \boldsymbol{n}; x', \boldsymbol{n}'; \boldsymbol{B}). \quad (23)$$

In the MRF, the elements of the type-II and type-III redistribution matrices are given by (see Equations (51) and (49) of Bommier 1997b, see also Equations (53) and (55) of Sampoorna 2011)

$$\boldsymbol{R}^{\rm II}_{ij}(x, \boldsymbol{n}, x', \boldsymbol{n}', \boldsymbol{B}) = \sum_{K'K''Q} (-1)^Q \mathcal{T}^{K''}_{Q}(i, \boldsymbol{n}) \mathcal{T}^{K'}_{-Q}(j, \boldsymbol{n}') \mathcal{R}^{K'',K'}_{Q,\rm II}(x, x', \Theta, B), \quad (24)$$

$$\boldsymbol{R}_{ij}^{\rm III}(x,\boldsymbol{n},x',\boldsymbol{n}',\boldsymbol{B}) = \sum_{KK'K''Q}(-1)^{Q}\mathcal{T}_{Q}^{K''}(i,\boldsymbol{n})\mathcal{T}_{-Q}^{K'}(j,\boldsymbol{n}')\mathcal{R}_{Q,\rm III}^{K'',K,K'}(x,x',\Theta,B). \tag{25}$$

In the above equations, i and j denote the Stokes parameter indices, which take values 0, 1, 2, and 3; $\mathcal{T}_{Q}^{K}(i,\boldsymbol{n})$ are the irreducible spherical tensors, where K takes values 0, 1, and 2, while Q varies in the range of $-K \leqslant Q \leqslant +K$ and $\boldsymbol{n}(\theta,\phi)$ refers to the ray direction with respect to the magnetic field; and Θ denotes the scattering angle between the incident and scattered rays. The laboratory frame redistribution functions $\mathcal{R}_{Q,\rm II}^{K'',K'}(x,x',\Theta,B)$ and $\mathcal{R}_{Q,\rm III}^{K'',K,K'}(x,x',\Theta,B)$ are given by

$$\begin{aligned}\mathcal{R}_{Q,\rm II}^{K'',K'}(x,x',\Theta,B) &= \frac{\Gamma_R}{\Gamma_R+\Gamma_I+\Gamma_E+i\omega_L g_{J_u}Q}3(2J_u+1)\\
&\times\sqrt{(2K'+1)(2K''+1)}\sum_{M_uM_u'M_lM_l'pp'p''p'''}(-1)^{J_u-M_l-1+Q}\\
&\times(-1)^{J_u-M_l'-1+Q}\begin{pmatrix}J_l & 1 & J_u\\ -M_l & -p & M_u\end{pmatrix}\begin{pmatrix}J_l & 1 & J_u\\ -M_l & -p' & M_u'\end{pmatrix}\\
&\times\begin{pmatrix}J_l & 1 & J_u\\ -M_l' & -p'' & M_u\end{pmatrix}\begin{pmatrix}J_l & 1 & J_u\\ -M_l' & -p''' & M_u'\end{pmatrix}\\
&\times\begin{pmatrix}1 & 1 & K'\\ -p & p' & Q\end{pmatrix}\begin{pmatrix}1 & 1 & K''\\ -p'' & p''' & Q\end{pmatrix}\\
&\times[h^{\rm II}_{M_uM_u'}(M_l'M_l)+{\rm i}f^{\rm II}_{M_uM_u'}(M_l'M_l)],\end{aligned} \tag{26}$$

$$\begin{aligned}\mathcal{R}_{Q,\rm III}^{K'',K,K'}(x,x',\Theta,B) &= \frac{\Gamma_R}{\Gamma_R+\Gamma_I+D^{(K)}+{\rm i}\omega_L g_{J_u}Q}\\
&\times\frac{[\Gamma_E-D^{(K)}]}{\Gamma_R+\Gamma_I+\Gamma_E+{\rm i}\omega_L g_{J_u}Q}3(2J_u+1)(2K+1)\\
&\times\sqrt{(2K'+1)(2K''+1)}\\
&\sum_{M_uM_u'M_u''M_u'''M_lM_l'pp'p''p'''}(-1)^{J_u-M_l-1+Q}(-1)^{J_u-M_l'-1+Q}\\
&\times\begin{pmatrix}J_l & 1 & J_u\\ -M_l & -p & M_u\end{pmatrix}\begin{pmatrix}J_l & 1 & J_u\\ -M_l & -p' & M_u'\end{pmatrix}\\
&\times\begin{pmatrix}J_l & 1 & J_u\\ -M_l' & -p'' & M_u''\end{pmatrix}\begin{pmatrix}J_l & 1 & J_u\\ -M_l' & -p''' & M_u'''\end{pmatrix}\\
&\times\begin{pmatrix}1 & 1 & K'\\ -p & p' & Q\end{pmatrix}\begin{pmatrix}1 & 1 & K''\\ -p'' & p''' & Q\end{pmatrix}\begin{pmatrix}J_u & J_u & K\\ M_u' & -M_u & Q\end{pmatrix}\\
&\times\begin{pmatrix}J_u & J_u & K\\ M_u''' & -M_u'' & Q\end{pmatrix}\frac{1}{4}[R^{\rm III,HH}_{M_u'M_l,M_u'''M_l'}+R^{\rm III,HH}_{M_u'M_l,M_u''M_l'}\\
&+R^{\rm III,HH}_{M_uM_l,M_u'''M_l'}+R^{\rm III,HH}_{M_uM_l,M_u''M_l'}+{\rm i}(R^{\rm III,FH}_{M_u'M_l,M_u'''M_l'}\\
&+R^{\rm III,FH}_{M_u'M_l,M_u''M_l'}-R^{\rm III,FH}_{M_uM_l,M_u'''M_l'}-R^{\rm III,FH}_{M_uM_l,M_u''M_l'})\\
&+{\rm i}(R^{\rm III,HF}_{M_u'M_l,M_u'''M_l'}-R^{\rm III,HF}_{M_u'M_l,M_u''M_l'}+R^{\rm III,HF}_{M_uM_l,M_u'''M_l'}\\
&-R^{\rm III,HF}_{M_uM_l,M_u''M_l'})-R^{\rm III,FF}_{M_u'M_l,M_u'''M_l'}+R^{\rm III,FF}_{M_u'M_l,M_u''M_l'}\\
&+R^{\rm III,FF}_{M_uM_l,M_u'''M_l'}-R^{\rm III,FF}_{M_uM_l,M_u''M_l'}].\end{aligned} \tag{27}$$

In the above equations, M_u, M_u', M_u'', M_u''' and M_l, M_l' denote the magnetic substates of the upper level J_u and the lower level J_l, respectively; $\omega_L = 2\pi\nu_L$ is the Larmor frequency, and g_{Ju} is the Landé factor of the upper level. Furthermore, Γ_R denotes the radiative de-excitation rate of the upper level, Γ_I the inelastic de-excitation rate, Γ_E the elastic collisional rate, and $D^{(K)}$ the depolarizing collisional rate. The auxiliary quantities corresponding to type-II redistribution are given by

$$\begin{aligned}h^{\rm II}_{M_uM_u'}(M_l'M_l) &= \frac{1}{2}[R^{\rm II,H}_{M_l'M_uM_l}+R^{\rm II,H}_{M_l'M_u'M_l}];\\
f^{\rm II}_{M_uM_u'}(M_l'M_l) &= \frac{1}{2}[R^{\rm II,F}_{M_l'M_u'M_l}-R^{\rm II,F}_{M_l'M_uM_l}],\end{aligned} \tag{28}$$

where the magnetic redistribution functions of type-II are given by

$$\begin{aligned}R^{\rm II,H}_{M_l'M_uM_l}(x,x',\Theta) &= \frac{1}{\pi\sin\Theta}\exp\left\{-\left[\frac{x-x'+x_{M_lM_l'}}{2\sin(\Theta/2)}\right]^2\right\}\\
&\times H\left(\frac{a}{\cos(\Theta/2)},\frac{x_{M_uM_l}+x'_{M_uM_l}+x_{M_lM_l'}}{2\cos(\Theta/2)}\right),\end{aligned} \tag{29}$$

$$\begin{aligned}R^{\rm II,F}_{M_l'M_uM_l}(x,x',\Theta) &= \frac{1}{\pi\sin\Theta}\exp\left\{-\left[\frac{x-x'+x_{M_lM_l'}}{2\sin(\Theta/2)}\right]^2\right\}\\
&\times F\left(\frac{a}{\cos(\Theta/2)},\frac{x_{M_uM_l}+x'_{M_uM_l}+x_{M_lM_l'}}{2\cos(\Theta/2)}\right).\end{aligned} \tag{30}$$

In the above equations, $H(a,x)$ and $F(a,x)$ are the Voigt and Faraday–Voigt functions, $x_{M_uM_l} = x + (g_{J_u}M_u - g_{J_l}M_l)(\nu_L/\Delta\nu_{\rm D})$ is the magnetically shifted non-dimensional frequency (with a similar expression for the primed quantity), $x_{M_lM_l'} = \nu_{M_lM_l'}/\Delta\nu_{\rm D}$ with $\nu_{M_lM_l'}$ being the energy difference between the magnetic substates M_l and M_l', and $a = (\Gamma_R+\Gamma_I+\Gamma_E)/(4\pi\Delta\nu_{\rm D})$ is the total damping width of the line. The magnetic redistribution functions of type-III appearing in Equation (27) are given by

$$\begin{aligned}R^{\rm III,HH}_{M_uM_l,M_u'M_l'}(x,x',\Theta) &= \frac{1}{\pi^2\sin\Theta}\int_{-\infty}^{+\infty}du\,e^{-u^2}\\
&\times\left[\frac{a}{a^2+(x'_{M_uM_l}-u)^2}\right]H\left(\frac{a}{\sin\Theta},\frac{x_{M_u'M_l'}}{\sin\Theta}-u\cot\Theta\right),\end{aligned} \tag{31}$$

$$\begin{aligned}R^{\rm III,HF}_{M_uM_l,M_u'M_l'}(x,x',\Theta) &= \frac{1}{\pi^2\sin\Theta}\int_{-\infty}^{+\infty}du\,e^{-u^2}\\
&\times\left[\frac{a}{a^2+(x'_{M_uM_l}-u)^2}\right]F\left(\frac{a}{\sin\Theta},\frac{x_{M_u'M_l'}}{\sin\Theta}-u\cot\Theta\right),\end{aligned} \tag{32}$$

$$\begin{aligned}R^{\rm III,FH}_{M_uM_l,M_u'M_l'}(x,x',\Theta) &= \frac{1}{\pi^2\sin\Theta}\int_{-\infty}^{+\infty}du\,e^{-u^2}\\
&\times\left[\frac{(x'_{M_uM_l}-u)}{a^2+(x'_{M_uM_l}-u)^2}\right]H\left(\frac{a}{\sin\Theta},\frac{x_{M_u'M_l'}}{\sin\Theta}-u\cot\Theta\right),\end{aligned} \tag{33}$$

and

$$R^{\rm III,FF}_{M_u M_l, M_u' M_l'}(x, x', \Theta) = \frac{1}{\pi^2 \sin\Theta} \int_{-\infty}^{+\infty} du\, e^{-u^2} \times \left[\frac{(x'_{M_u M_l} - u)}{a^2 + (x'_{M_u M_l} - u)^2}\right] F\left(\frac{a}{\sin\Theta}, \frac{x_{M_u' M_l'}}{\sin\Theta} - u\cot\Theta\right). \quad (34)$$

Following Section 5.12 of Landi Degl'Innocenti & Landolfi (2004, see also Frisch 2007), we transform Equations (24) and (25) to the ARF. In the ARF, the magnetic field makes an angle ϑ_B with the atmospheric normal and has an azimuth φ_B. The elements of the type-II and type-III redistribution matrices in ARF are given by

$$\boldsymbol{R}^{\rm II}_{ij}(x, \boldsymbol{n}, x', \boldsymbol{n}', \boldsymbol{B}) = \sum_{K''Q} \mathcal{T}^{K''}_{Q}(i, \boldsymbol{n}) \times \sum_{K'Q'} N^{K'',K'}_{QQ',\rm II}(x, x', \Theta, \boldsymbol{B})(-1)^{Q'} \mathcal{T}^{K'}_{-Q'}(j, \boldsymbol{n}'), \quad (35)$$

$$\boldsymbol{R}^{\rm III}_{ij}(x, \boldsymbol{n}, x', \boldsymbol{n}', \boldsymbol{B}) = \sum_{K''Q} \mathcal{T}^{K''}_{Q}(i, \boldsymbol{n}) \times \sum_{KK'Q'} N^{K'',K,K'}_{QQ',\rm III}(x, x', \Theta, \boldsymbol{B})(-1)^{Q'} \mathcal{T}^{K'}_{-Q'}(j, \boldsymbol{n}'), \quad (36)$$

where $\boldsymbol{n}(\vartheta, \varphi)$ and $\boldsymbol{n}'(\vartheta', \varphi')$ now refer to the ray directions with respect to the atmospheric normal. The type-II and type-III magnetic kernels have the form

$$N^{K'',K'}_{QQ',\rm II}(x, x', \Theta, \boldsymbol{B}) = e^{{\rm i}(Q'-Q)\varphi_B} \times \sum_{Q''} d^{K''}_{QQ''}(\vartheta_B) d^{K'}_{Q''Q'}(-\vartheta_B) \mathcal{R}^{K'',K'}_{Q'',\rm II}(x, x', \Theta, B), \quad (37)$$

$$N^{K'',K,K'}_{QQ',\rm III}(x, x', \Theta, \boldsymbol{B}) = e^{{\rm i}(Q'-Q)\varphi_B} \times \sum_{Q''} d^{K''}_{QQ''}(\vartheta_B) d^{K'}_{Q''Q'}(-\vartheta_B) \mathcal{R}^{K'',K,K'}_{Q'',\rm III}(x, x', \Theta, B). \quad (38)$$

Explicit forms of the reduced rotation matrices $d^{K}_{QQ'}(\vartheta_B)$ are given in Table 2.1 of Landi Degl'Innocenti & Landolfi (2004).

Appendix B
The Zeeman Line Absorption Matrix

For a two-level atom with an unpolarized lower level, the explicit form of the Zeeman line absorption matrix is given in Stenflo (1994) and Landi Degl'Innocenti & Landolfi (2004). However, this matrix is usually given in a frame where the magnetic field is along the Z-axis. For the problem at hand, it is necessary to transform this matrix to the ARF. For clarity, we present such a transformation in this appendix using the irreducible spherical tensors for polarimetry.

The Zeeman line absorption matrix has the form

$$\boldsymbol{\Phi} = \begin{bmatrix} \varphi_I & \varphi_Q & \varphi_U & \varphi_V \\ \varphi_Q & \varphi_I & \chi_V & -\chi_U \\ \varphi_U & -\chi_V & \varphi_I & \chi_Q \\ \varphi_V & \chi_U & -\chi_Q & \varphi_I \end{bmatrix}. \quad (39)$$

The absorption coefficients, φ_i with $i = 0, 1, 2, 3$ (corresponding to Stokes parameters I, Q, U, and V) may be written as (see Equation (A13.9) of Landi Degl'Innocenti & Landolfi 2004)

$$\varphi_i = \sum_K \mathcal{T}^K_0(i, \boldsymbol{n}) \Phi^{0K}_0(J_l, J_u, x), \quad (40)$$

where $\boldsymbol{n}(\theta, \phi)$ is the angle between the line of sight and the magnetic field, and the generalized profile function is given by (see Landi Degl'Innocenti et al. 1991)

$$\Phi^{0K}_0(J_l, J_u, x) = \sum_{M_u M_l q} (-1)^{q-1} \sqrt{3(2K+1)} \times \begin{pmatrix} J_u & J_l & 1 \\ -M_u & M_l & q \end{pmatrix}^2 \begin{pmatrix} 1 & 1 & K \\ -q & q & 0 \end{pmatrix} H(a, x_{M_u M_l}). \quad (41)$$

The anomalous dispersion coefficients, χ_i with $i = 1, 2, 3$ (corresponding to Stokes parameters Q, U, and V) may be written as (see Equation (A13.14) of Landi Degl'Innocenti & Landolfi 2004)

$$\chi_i = \sum_K \mathcal{T}^K_0(i, \boldsymbol{n}) \Psi^{0K}_0(J_l, J_u, x), \quad (42)$$

where the generalized dispersion profile function is given by (see Landi Degl'Innocenti et al. 1991)

$$\Psi^{0K}_0(J_l, J_u, x) = \sum_{M_u M_l q} (-1)^{q-1} \sqrt{3(2K+1)} \times \begin{pmatrix} J_u & J_l & 1 \\ -M_u & M_l & q \end{pmatrix}^2 \begin{pmatrix} 1 & 1 & K \\ -q & q & 0 \end{pmatrix} F(a, x_{M_u M_l}). \quad (43)$$

Equations (40) and (42) refer to the absorption and dispersion coefficients in the MRF. They can be transformed to the ARF using the rotation law obeyed by the irreducible spherical tensors. From Equation (2.78) of Landi Degl'Innocenti & Landolfi (2004), we can write

$$[\mathcal{T}^K_Q(i, \boldsymbol{n})]_{\rm MRF} = \sum_{Q'} [\mathcal{T}^K_{Q'}(i, \boldsymbol{n})]_{\rm ARF} D^K_{QQ'}(0, -\vartheta_B, -\varphi_B)^*, \quad (44)$$

where $D^K_{QQ'}$ are the Wigner rotation matrices. Using this transformation law, we obtain the absorption and dispersion coefficients in the ARF as

$$\varphi_i = \sum_{KQ} \mathcal{T}^K_Q(i, \boldsymbol{n}) e^{-{\rm i}Q\varphi_B} d^K_{Q0}(\vartheta_B) \Phi^{0K}_0(J_l, J_u, x), \quad (45)$$

$$\chi_i = \sum_{KQ} \mathcal{T}^K_Q(i, \boldsymbol{n})\, e^{-{\rm i}Q\varphi_B} d^K_{Q0}(\vartheta_B) \Psi^{0K}_0(J_l, J_u, x), \quad (46)$$

where $\boldsymbol{n}(\vartheta, \varphi)$ now refers to the angle made by the line of sight with respect to the ARF.

Appendix C
Normalization of the Hanle–Zeeman Redistribution Matrix

As shown in Bommier (2017), the Hanle–Zeeman redistribution matrix is normalized to

$$\int dx \int dx' \oint \frac{d\boldsymbol{n}}{4\pi} \oint \frac{d\boldsymbol{n}'}{4\pi} \boldsymbol{R}_{ij}(x, \boldsymbol{n}; x', \boldsymbol{n}'; \boldsymbol{B}) = \delta_{i0}\delta_{j0} \frac{\Gamma_R}{\Gamma_R + \Gamma_I}. \quad (47)$$

For accurate evaluation of the scattering integral, namely $\boldsymbol{S}_{\rm scat}$, it is absolutely essential to correctly normalize the Hanle–Zeeman redistribution matrix, particularly when angle-dependent

redistribution functions are used. To achieve this numerically, we first analytically derive the normalization of the type-II and type-III redistribution matrices by integrating only over the incoming angles and frequencies. The resulting analytic expressions (given below) are used to re-normalize the redistribution matrices that are numerically computed. From Equation (47), it is clear that such a re-normalization is effective only for the $\boldsymbol{R}_{00}$ element.

We analytically integrate Equations (35)–(38) over the incoming angles $\boldsymbol{n}'$ and frequencies x' and obtain

$$\int dx' \oint \frac{d\boldsymbol{n}'}{4\pi} \boldsymbol{R}_{00}^{\rm II}(x, \boldsymbol{n}; x', \boldsymbol{n}'; \boldsymbol{B}) = \frac{\Gamma_R}{\Gamma_R + \Gamma_I + \Gamma_E} \times \sum_{K''Q} \mathcal{T}^{K''}_{Q}(0, \boldsymbol{n}) e^{-{\rm i}Q\varphi_B} d^{K''}_{Q0}(\vartheta_B)(2J_u + 1)\sqrt{3(2K'' + 1)} \times \sum_{M_u M_l M_l' pp''} (-1)^{1+p''} \begin{pmatrix} J_l & 1 & J_u \\ -M_l & -p & M_u \end{pmatrix}^2 \begin{pmatrix} J_l & 1 & J_u \\ -M_l' & -p'' & M_u \end{pmatrix}^2 \times \begin{pmatrix} 1 & 1 & K'' \\ -p'' & p'' & 0 \end{pmatrix} H(a, x_{M_u M_l} + x_{M_l M_l'}), \quad (48)$$

for the type-II redistribution and

$$\int dx' \oint \frac{d\boldsymbol{n}'}{4\pi} \boldsymbol{R}_{00}^{\rm III}(x, \boldsymbol{n}; x', \boldsymbol{n}'; \boldsymbol{B}) = \frac{\Gamma_R}{\Gamma_R + \Gamma_I} \frac{\Gamma_E}{\Gamma_R + \Gamma_I + \Gamma_E} \times \sum_{K''Q} \mathcal{T}^{K''}_{Q}(0, \boldsymbol{n}) e^{-{\rm i}Q\varphi_B} d^{K''}_{Q0}(\vartheta_B) \sqrt{3(2K'' + 1)} \times \sum_{M_u M_l p} (-1)^{1+p} \begin{pmatrix} J_l & 1 & J_u \\ -M_l & -p & M_u \end{pmatrix}^2 \begin{pmatrix} 1 & 1 & K'' \\ -p & p & 0 \end{pmatrix} H(a, x_{M_u M_l}), \quad (49)$$

for the type-III redistribution. When deriving the above equations, we have made use of the normalization property of the irreducible spherical tensors for polarimetry (see Landi Degl'Innocenti 1984, see also Equation (27) of Bommier 2017). If we further integrate Equations (48) and (49) over the outgoing angles $\boldsymbol{n}$ and frequencies x, we obtain $\Gamma_R/(\Gamma_R + \Gamma_I + \Gamma_E)$ for the type-II redistribution and $[\Gamma_R/(\Gamma_R + \Gamma_I)] \times [\Gamma_E/(\Gamma_R + \Gamma_I + \Gamma_E)]$ for the type-III redistribution, which when added gives the right-hand side of Equation (47).

References

Alsina Ballester, E., Belluzzi, L., & Trujillo Bueno, J. 2016, ApJL, 831, L15
Alsina Ballester, E., Belluzzi, L., & Trujillo Bueno, J. 2017, ApJ, 836, 6
Bommier, V. 1997a, A&A, 328, 706
Bommier, V. 1997b, A&A, 328, 726
Bommier, V. 2017, A&A, in press
Bommier, V., & Stenflo, J. O. 1999, A&A, 350, 327
Cannon, C. J. 1973, ApJ, 185, 621
Dumont, S., Omont, A., Pecker, J. C., & Rees, D. E. 1977, A&A, 54, 675
Faurobert, M. 1987, A&A, 178, 269
Frisch, H. 2007, A&A, 476, 665
Landi Degl'Innocenti, E. 1984, SoPh, 91, 1
Landi Degl'Innocenti, E., Bommier, V., & Sahal-Bréchot, S. 1991, A&A, 244, 391
Landi Degl'Innocenti, E., & Landolfi, M. 2004, Polarization in Spectral Lines (Dordrecht: Kluwer)
Mihalas, D. 1978, Stellar Atmosphere (2nd ed.; San Francisco, CA: Freeman)
Nagendra, K. N. 1986, PhD thesis, Bangalore Univ.
Nagendra, K. N. 1988, ApJ, 335, 269
Nagendra, K. N. 2017, in ASP Conf. Ser., Solar Polarization 8, ed. L. Belluzzi et al. (San Francisco, CA: ASP), in press
Nagendra, K. N., Frisch, H., & Faurobert, M. 2002, A&A, 395, 305
Nagendra, K. N., Paletou, F., Frisch, H., & Faurobert-Scholl, M. 1999, in Solar Polarization, ed. K. N. Nagendra & J. O. Stenflo (Boston, MA: Kluwer), 127
Nagendra, K. N., & Sampoorna, M. 2011, A&A, 535, A88
Olson, G. L., Auer, L. H., & Buchler, J. R. 1986, JQSRT, 35, 431
Rees, D. E., & Saliba, G. J. 1982, A&A, 115, 1
Sampoorna, M. 2011, ApJ, 731, 114
Sampoorna, M. 2014, in ASP Conf. Ser., 489, Solar Polarization 7, ed. K. N. Nagendra et al. (San Francisco, CA: ASP), 197
Sampoorna, M., Nagendra, K. N., & Stenflo, J. O. 2007a, ApJ, 663, 625
Sampoorna, M., Nagendra, K. N., & Stenflo, J. O. 2007b, ApJ, 670, 1485
Sampoorna, M., Nagendra, K. N., & Stenflo, J. O. 2008, ApJ, 679, 889
Stenflo, J. O. 1994, Solar Magnetic Fields: Polarized Radiation Diagnostics (Dordrecht: Kluwer)
Stenflo, J. O. 2013, A&ARv, 21, 66
Supriya, H. D., Sampoorna, M., Nagendra, K. N., Ravindra, B., & Anusha, L. S. 2013, JQSRT, 119, 67
Trujillo Bueno, J. 2003, in ASP Conf. Ser. 288, Stellar Atmosphere Modeling, ed. I. Hubeny, D. Mihalas, & K. Werner (San Francisco, CA: ASP), 551
Trujillo Bueno, J., & Manso Sainz, R. 1999, ApJ, 516, 436